energies

MDPI

Article

Grid-Forming Operation of Energy-Router Based on Model Predictive Control with Improved Dynamic Performance

Mahdieh Najafzadeh [1], Natalia Strzelecka [2,*], Oleksandr Husev [1], Indrek Roasto [1], Kawsar Nassereddine [3], Dmitri Vinnikov [1] and Ryszard Strzelecki [4]

[1] Department of Electrical Power Engineering and Mechatronics, Tallinn University of Technology, 19086 Tallinn, Estonia; mahdieh.najafzadeh@taltech.ee (M.N.); oleksandr.husev@taltech.ee (O.H.); indrek.roasto@ieee.org (I.R.); dmitir.vinnikov@taltech.ee (D.V.)
[2] Faculty of Electrical Engineering, Gdynia Maritime University, 81-225 Gdynia, Poland
[3] Faculty of Engineering, Lebanese University, Beirut 6573, Lebanon; nassereddinejana@gmail.com
[4] Faculty of Electrical and Control Engineering, Gdańsk University of Technology, 80-233 Gdańsk, Poland; ryszard.strzelecki@pg.edu.pl
* Correspondence: n.strzelecka@we.umg.edu.pl

Abstract: The focus of this study is on the grid-forming operation of the Energy Router (ER) based on Model Predictive Control (MPC). ER is regarded as a key component of microgrids. It is a converter that interfaces the microgrid (s) with the utility grid. The ER has a multiport structure and bidirectional energy flow control. The ER concept can be implemented in Nearly Zero-Energy Buildings (NZEB) to provide flexible energy control. A concept is proposed where the ER works as a single grid-forming converter. The challenge is to keep the predefined reference voltage and frequency inside the NZEB in all possible modes, including the idle operation mode, current sources, and nonlinear load control. To gain stability and output voltage quality, the MPC is proposed. The design of the modified MPC algorithm with improved dynamics performance is explained. PLECS software is utilized to verify the proposed algorithm. The results demonstrate the suitable performance of the proposed control method in terms of total harmonic distortion of the output voltage. The influence of weighting coefficiencies is evaluated, showing the higher impact of the capacitor filter voltage on lowering the total harmonics distortion of the output voltage. Finally, the capability of the control system toward step change in the reference value is evaluated.

Keywords: energy router; current sources; nonlinear load; grid-forming control; bidirectional power flow control; model predictive control

Citation: Najafzadeh, M.; Strzelecka, N.; Husev, O.; Roasto, I.; Nassereddine, K.; Vinnikov, D.; Strzelecki, R. Grid-Forming Operation of Energy-Router Based on Model Predictive Control with Improved Dynamic Performance. *Energies* **2022**, *15*, 4010. https://doi.org/10.3390/en15114010

Academic Editor: Nicu Bizon

Received: 24 April 2022
Accepted: 26 May 2022
Published: 30 May 2022

1. Introduction

The steadily increasing penetration of renewable energy sources (RESs) in the utility grid is a current trend [1,2], which, in turn, is a source of many technical challenges that need to be overcome. The voltage/frequency disturbances caused by the chaotic nature of RES in the utility grid are widely known.

The solution is to shift the responsibility to the local prosumer. Accordingly, in many countries, governments have set strict regulations on grid energy injection. This consists of the limitations of the power injected into the grid produced by RES in local households. Near Zero-Energy Building (NZEB) is a concept regarding reductions in energy consumption in households. This is achieved in several ways, including energy-saving technologies, modern heating systems, and modern power electronics facilities. New power electronics facilities ensure zero energy consumption by means of energy flow control between RESs, storage batteries and loads. The announced priorities are drifting from mass RESs used for grid balancing.

A more recent concept is the so-called smart communities, which take advantage of the Smart Grid (SG), allowing for effective demand-side management. SGs require

general-purpose power electronic converters (in both dc and ac), micro-storage systems installed at the residential level, advanced metering infrastructure, and the optimal use of information and communication technology [3]. In this regard, the trend moves toward the concept of energy routers (ERs) or hubs [4].

The concept of ER, introduced by the NSF FREEDM Systems Center in 2010 [2], introduces an SST-based ER concept and describes the IoE architecture. In this way, a flexible and two-directional energy flow will be the future of the distribution network [5,6]. The main tool is the ER, which manages the power flow between the subnet, main grid, RESs and other components. The further development of the concept for microgrids application is addressed in many papers. Complementary energy exchange by means of ER between neighboring microgrids is addressed in [6,7]. The control strategy of ER inside a microgrid with different energy sources, loads and battery ES is studied in [8]. Work [9] studied the utilization of a hybrid converter as an ER in a case of dc nanogrid. The conceptual architecture of the ER in a residential application and different power-electronics architectures are discussed in [4]. Finally, paper [10] is devoted to the ER as a power management tool in the case of low-voltage residential applications. The further extension of this approach consists of ER utilization for the NZEB concept. It has to provide flexible energy management in the case of different loads, energy sources, and battery storage. In advance of the grid-connected mode, the islanded mode, when the main grid is disconnected, has to be realized. In conclusion, the NZEB corresponds to the hybrid nanogrid [11,12], while the goal of the ER is to maintain a stable output voltage in all operation modes. Active and reactive power control, voltage control, current control, and protection functions are just a few of the active functions that an ER could have [4].

Figure 1 shows a single-phase multiport converter topology that is selected to realize the interface between the external grid and internal load. Inherently, it has dc and ac terminals, which make similar micro-and nanogrids converters [13]. Two dc–dc interface converters allow for energy storage and local energy generation sources to be connected. In addition, dc loads can be connected to the dc-port. The different dc-load connection to the dc-port of the ER and the proposed control technique is studied in [14]. The output ac port is directly connected to the house appliances. Appliances in the NZEB are considered as "grid followers", only. At the same time, it is well-known that diferent types of load have to be considered, including light load and non-linear loads. The basic operation modes of the considered ER are described in [15]. This work studies the quality of the grid-forming operation in extremely nonlinear conditions and small current sources. Enhancing the classic linear controller to nonlinear control technique (MPC) and, specifically, the cost function of the proposed MPC with the filter capacitor voltage of the output side is the main contribution of this work. The next section concentrates on the conventional grid-following solution and the limitations of the conventional control system. The proposed indirect MPC is explained in the following sections. Finally, the parameter selections and the simulation results for different scenarios are described. The robustness test results in case of a drop in the reference voltage are also demonstrated.

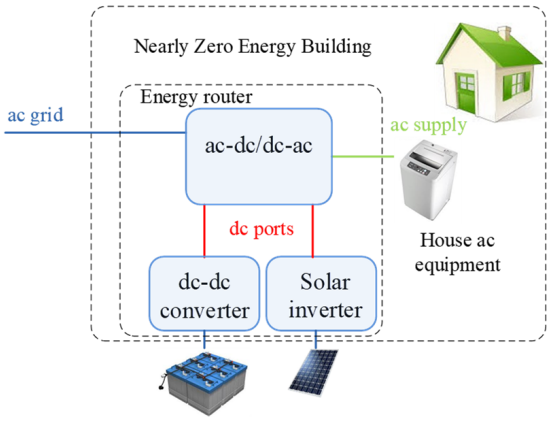

Figure 1. Energy router for NZEB.

2. Conventional Grid-Forming Control Systems and Problem Definition

Figure 2 shows the electrical circuit diagram of the ER. The measured signals are marked in red. One of the conventional control systems of the ER is shown in Figure 3. It has a conventional Phase-Locked Loop (PLL) block that provides synchronization to the primary grid [16]. The traditional Second-Order Generalized Integrator (SOGI) regulator is used [17]. The grid side reference current is derived by means of a simple proportional-integral (PI) controller, in combination with the instantaneous value of the output current. This provides the instantaneous power balance between the output side and the grid side, which, in turn, mitigates the power ripple across the dc-link capacitor and improves the dynamic of the system. Finally, a conventional proportional-resonant (PR) controller is used for grid current control. Thus, the grid-side control operation is ensured (Figure 3a).

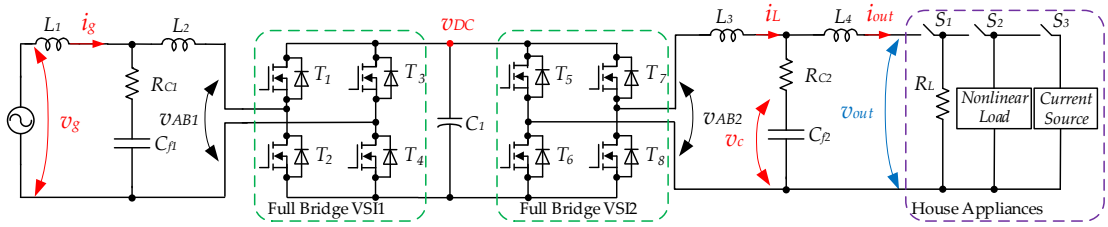

Figure 2. Back-to-back mode circuit diagram of the proposed energy router.

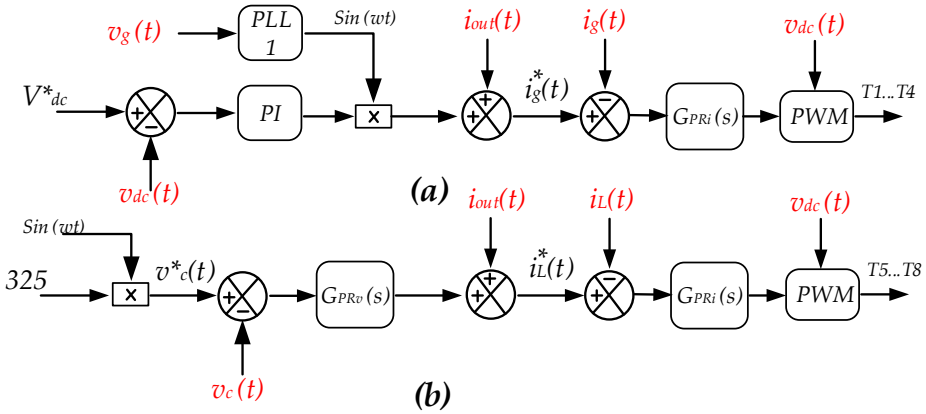

Figure 3. The conventional control system structure of the ER primary grid-side VSI1 control (**a**) and output side grid-forming VSI2 control (**b**).

The PR controller is a key element of the discussed grid-side control system. To provide the proper dynamic, it has to be the fastest and most properly tuned chain in the control loop [18].

The output control has a more complex structure. The classical definition of the grid-forming operation is derived from the microgrid application and has high-level and low-level control components. The low-level algorithm has to provide the output voltage according to the reference value. An example of the output voltage control structure is illustrated in Figure 3b. The initial goal of the output side controller is to provide sinusoidal output voltage under any output load. As a result, a consumer recognizes this as a normal grid. It typically has current and voltage control loops [19–23]. The internal structure can differ. In the three-phase system, the dq rotating frame is often used, while resonant controllers are mostly used for a single-phase system. In both cases, the most attention should be paid to the stable operation of the system. The current control loop is usually tuned as a fast control loop, while the voltage control loop has a damped dynamic.

The high-level algorithm provides the power-sharing control in the case of several power sources working in parallel. First and foremost, this is achievable through Droop control [24–28]. It is a well-known and verified approach.

The virtual impedance [29,30] method and its derivation can also be applied for this purpose. Finally, a relatively novel approach, based on the synchronverter concept, was proposed in [31–33]. The goal of a high-level algorithm is to provide different amplitudes and frequencies of the reference voltage across the filter capacitor. It enables the stable operation of the microgrid. However, this is beyond the scope of this work.

In the classical approach, the voltage at the Point of Common Coupling (PCC) is not under direct control. It is assumed that only linear loads with sinusoidal current sources can be connected to the PCC. At the same time, it is obvious that this assumption is not acceptable in household applications where ER is connected to different low-power loads and current sources. It is clear that the PCC obtains higher harmonics from appliances such as solar microinverters and other nonlinear loads and current sources.

This paper is focused on how to improve the voltage shape in the PCC when the ER is used with different loads and current sources. In addition, the robustness of the system toward external noises and perturbations is another criterion that should be considered. Different control methods were studied to compensate the system disturbances [34,35]. In this paper, the ER control robustness is evaluated in the final step.

3. Grid-Forming Operations Based on Indirect Model Predictive Control

Model Predictive Control (MPC) is a well-known approach in power electronics from the 1980s [36]. Despite the complexity of the MPC, which imposes limitations on its utilization in power electronics, the progress of computational resources makes it increasingly feasible for industrial applications [37,38]. According to the most recent research, this can be used in a variety of power electronics fields [39–47]. MPC is categorized into two types: Finite Control Set (FCS) MPC and Continuous Control Set (CCS) MPC. FCS MPC provides optimized switching states; as a result, it can provide a variable switching frequency, resulting in higher THD [48]. On the other hand, CCS MPC produces the required duty cycles for modulators with a fixed switching frequency, ending with a lower THD [40,49]. Considering the priority of a lower THD in the grid forming operation, CCS MPC matches our control application.

Figure 4 shows the proposed control system. The control system for the primary side of the ER is shown in Figure 4a. Only one modification concerns an additional PLL block. It provides a pure sinusoidal reference current that is equal to the fundamental harmonic of the output current. It will provide only a sinusoidal grid current under any shape of the output current. All non-active harmonics will be circulated between the DC-link and the secondary side of the ER.

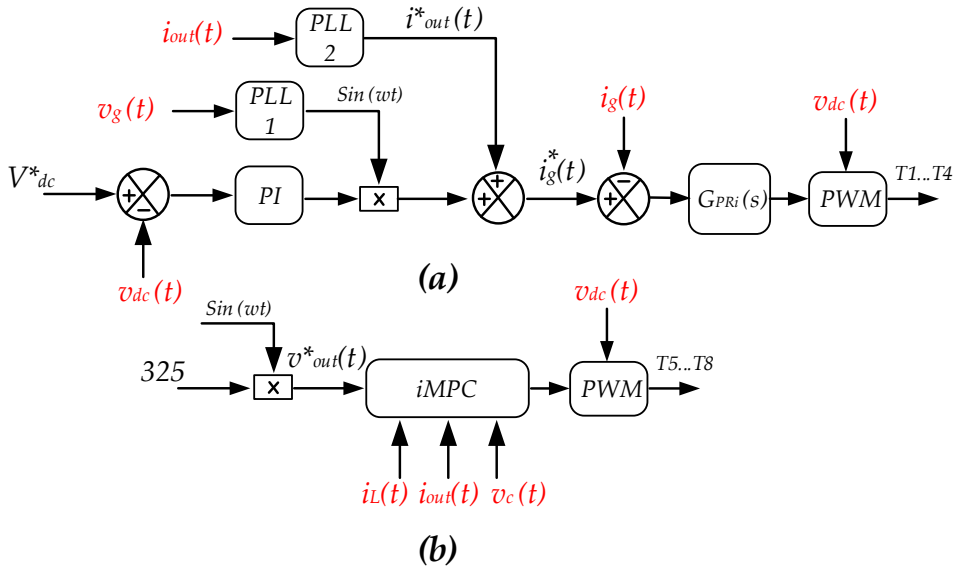

Figure 4. The proposed control system structure of the ER primary grid-side VSI1 control (**a**) and output side grid-forming VSI2 control (**b**).

Figure 4b shows the part of the control system that is formed in response to the grid-forming operation. In a very general case, the MPC says what the control action should be by trying to minimize: a cost function that describesthe target of the control system.

The proposed approach was partially studied in [50] for the unidirectional power flow control mode. In our case, the main goal of the proposed control system was to maintain the output voltage shape according to the reference sinusoidal signal under any type of load or current source that can be connected from the house side. Different from the classical approach, where only the voltage across the filter capacitor is controlled, MPC allows for control of both voltages across the capacitor and the output voltage, even without direct measurement of the last value. It turns out that, in our case, the cost function J is defined as:

$$J\,[d] = k_{out}|\Delta v_{out}(n+1)| + k_c|\Delta v_c(n+1)| + \ldots + k_{out}|\Delta v_{out}(n+p)| + k_c|\Delta v_c(n+p)| \quad (1)$$

It contains a voltage error across the filter capacitor and an error of the output voltage, along with corresponding weighting coefficients. It also has p elements that are defined by horizon prediction. The function quantizes the estimations of different summarized outputs and capacitor voltage errors. Each of those estimations corresponds to the possible scenario d, which could occur at the prediction horizon.

The measurement system provides the dc-link voltage, the voltage across the filter capacitor and currents in the inductors. If you want to conduct any more calculations, you need to use the indirect MPC and the dynamic model of the system shown in Figure 5.

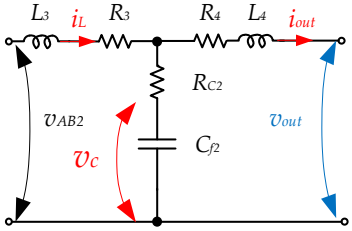

Figure 5. The dynamic model of the secondary side part of the ER used for iMPC.

The dynamic system is represented by the continuous vector of the measured parameters:

$$x(t) = [\, i_L(t), i_{out}(t),\, v_c(t)]^T, \quad (2)$$

After the measured signal discretization, the discontinuous set of the measured values is derived:

$$x(i) = [\, i_L(i), i_{out}(i),\ v_c(i)]^T, \tag{3}$$

After obtaining the measured values, the first step is to calculate the voltage at the PCC point based on a simple equation:

$$v_{out}(n\,) = v_c(n\,) - (i_L(n) - i_{out}(n)) \times R_{C2} - \frac{L_3}{T_S}(i_{out}(n) - i_{out}(n-1)) - R_4 \times i_{out}(n), \tag{4}$$

where T_S is the sampling time, L_3, L_4, C_{f2} are parameters of the output filter, R_3, R_4, R_{C2} are parasitic resistances.

To calculate the grid current value during the next samples in the discrete-time domain:

$$x(n+1) = F{\cdot}x(n) + G\,u(n), \tag{5}$$

$$\mathrm{u}(n) = [\, v_{AB}(n),\ v_{out}(n)\,]^T \tag{6}$$

where F and G are matrices that correspond to the dynamic model of the system and sampling frequency:

$$F = \begin{bmatrix} f_1 & f_2 & f_3 \\ f_4 & f_5 & f_6 \\ f_7 & f_8 & f_9 \end{bmatrix}, \tag{7}$$

$$G = \begin{bmatrix} g_1 & 0 \\ 0 & g_4 \\ 0 & 0 \end{bmatrix}, \tag{8}$$

$$f_1 = 1 - (R_3 + R_{C2})\frac{T_S}{L_3}; f_2 = \frac{R_{C2}T_S}{L_3}; f_3 = -\frac{T_S}{L_3}; \tag{9}$$

$$f_4 = \frac{R_{C2}T_S}{L_4}; f_5 = 1 - (R_4 + R_{C2})\frac{T_S}{L_4}; f_6 = \frac{T_S}{L_4}; \tag{10}$$

$$f_7 = \frac{T_S}{C_{f2}}; f_8 = -\frac{T_S}{C_{f2}}; f_9 = 1; \tag{11}$$

$$g_1 = \frac{T_S}{L_3}; g_4 = -\frac{T_S}{L_4}, \tag{12}$$

The proposed approach provides us a reference output voltage in the PCC. To make sure the control system works properly, the voltage across the capacitor is set as follows:

$$v_c^*(t) = v_{out}^*(t) - (i_L(t) - i_{out}^*(t)) \times R_{C2} + L_4\frac{d}{dt}i_{out}^*(t) + R_4 \times i_{out}^*(t), \tag{13}$$

In the further step, the voltage across the capacitor of the output filter is calculated as a function of the applied inverter voltage. The same concerns the output voltage in the PCC, which can be estimated similarly to Equation (4). As a result, the proposed control system keeps the capacitor voltage and the voltage in the PCC under control, considering the difference between them.

Finally, possible errors are calculated:

$$\Delta v_{out}(n+1) = v_{out}(n+1) - v_{out}^*(n+1);\ \Delta v_c(n+1) = v_c(n+1) - v_c^*(n+1); \tag{14}$$

The flow chart diagram for the case $p = 2$ is shown in Figure 6. Firstly, the variables are measured, and then the output voltage is estimated.

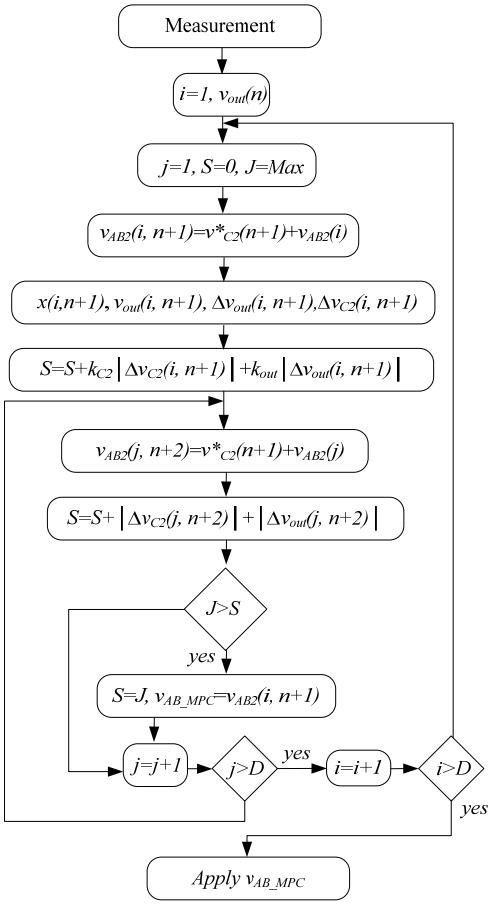

Figure 6. The procedure of activity diagram of the proposed iMPC in the case of $p = 2$.

Based on this estimated state, the predicted state of the system at $n + 1$ is calculated for all the possible output inverter values v_{AB2} combinations.

It should be mentioned that, in any case, the output inverter voltage is expected to be close to the sinusoidal reference signal. $v_{AB2(i)}$ is an example of a possible reference voltage that could be used to figure out the cost function:

$$v_{AB2}(n+1) = v_c^*(n+1) + \Delta v_{AB2}(i), \tag{15}$$

Finally, the combination of voltages on the output inverter that minimizes (1) is stored and will be used at the start of the next test.

4. Optimal Parameters Selection

The main criterion for the quality evaluation of the output voltage is the THD. At the same time, from the above description, it is evident that the resulting THD depends on the horizon prediction p, weighting coefficients, and the voltage quantizing d. Due to the nonlinearity of the control, the most suitable tuning approach is achieved by simulation. In this work, the PLECS simulation tool was used as the simulation environment.

The parameters of the prototype are shown in Table 1. They are used for simulation and experimental tests.

Table 1. Components and parameters of the ER.

Parameter	Value
Input RMS ac voltage V_{IN}	230 V
Output ac RMS voltage V_{OUT}	230 V
Output power	0.3–3.6 kW
Dc-link capacitor C_1	0.8 mF
Grid side inductor filter L_1	0.6 mH
Grid side second inductor filter L_2	1.44 mH
Grid side capacitor filter C_{f1} R_{C1}	3 µF, 0.8 Ohm
Output side inductor filter L_3	1.44 mH
Output side second inductor filter L_4	0.6 mH
Output side capacitor filter C_{f2} R_{C2}	9.6 µF, 0.8 Ohm
Switching frequency f	25 kHz
Sampling frequency f	25 kHz

First of all, based on previous research [50], it is assumed that the horizon prediction $p = 2$ is optimal. Increasing p even more will not make a big difference in THD, but it will make the calculations a lot more complicated. According to Equation (15), the output voltage value is selected, close to the present reference voltage value with respect to voltage deviations. During each sampling, five possible output voltage deviation values are individually considered and verified. This number is constant from sample to sample, which is limited by the calculation resources. However, the possible minimum and maximum values can be different:

$$-\Delta v_{AB2\_max} < \Delta v_{AB2}(i,d) < \Delta v_{AB2\_max}, \tag{16}$$

It is well known that the voltage difference between the filter capacitor and the PCC is defined by the parasitic resistance R_4 (Figure 5), inductance L_4 and current. The maximum and minimum voltages that can be applied to the inverter can be flexible and changed slightly based on the peak current.

In conclusion, the most significant parameters for evaluation are the weighting coefficients. The idea of these coefficients consists of a priority setting between the quality of the output capacitor voltage and the quality of the PCC voltage. On the one hand, it is evident that the PCC is more important than the voltage across the capacitor, which is an internal parameter. However, this parameter that can be directly measured, and direct control of it could improve both the capacitor and the PCC.

A simulation was performed to study the influence of these coefficients. Figure 7 shows the simulation results in the case of $k_{out} = 0$, $k_c = 1$. This means that only the quality of the capacitor voltage is considered in the cost function estimation. At the very beginning, the DC-link is charged and a 529 W simple resistive load is connected at 0.25 s. At 0.35 s, the nonlinear 180 W load is connected. To emulate a highly nonlinear load, a resistor with a half-bridge diode with an LC filter is assumed. It can be seen that, at the resistive load, both the capacitor and the PCC voltage have a good shape, without significant distortions. At the nonlinear load connection, both voltages have distortions. However, it is evident that the capacitor voltage is less distorted. The grid current is also distorted by the nonlinear load connection.

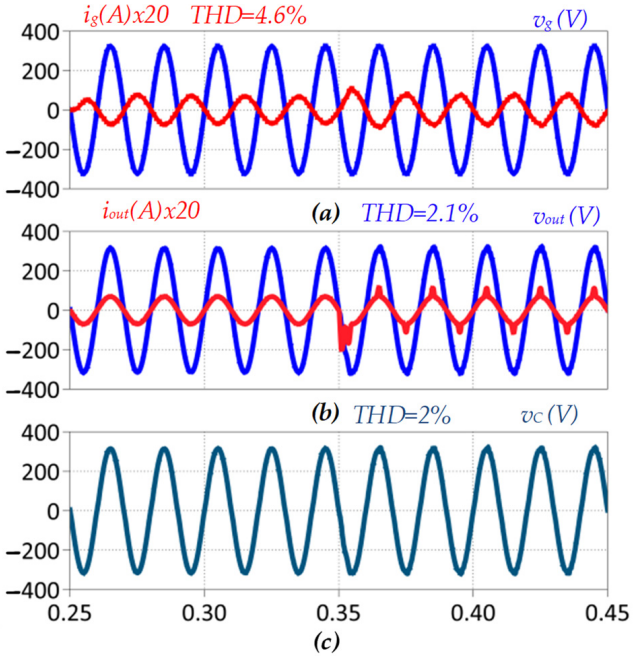

Figure 7. Voltage and current shape at the main grid (**a**), output (**b**), and capacitor of the filter (**c**) with $k_{out} = 0$, $k_c = 1$.

The opposite situation is shown in Figure 8. In this case, the predicted capacitor voltage is not considered in the cost function estimation. It can be seen from Figure 8 that with a simple resistive load, the quality of the PCC voltage and the capacitor voltage is good, but the situation changes under a nonlinear load. Both shapes are more distorted compared to Figure 7 results. However, the THD of the grid current remains constant.

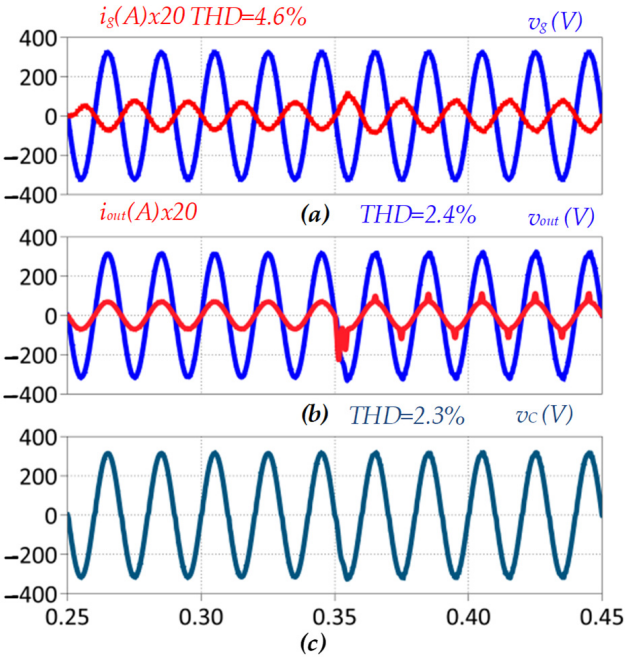

Figure 8. Voltage and current shape at the main grid (**a**), output (**b**), and capacitor of the filter (**c**) with $k_{out} = 1$, $k_c = 0$.

The simulation results of different coefficients k_{out}, k_c show the influence of the weighting coefficients k_{out}, k_c on the THD of output voltage and capacitor voltage. It is assumed that $k_{out} + k_c = 1$ under nonlinear load. The results show that different values of k_{out} and

k_c have no significant impact on THD, but lower k_{out} improves the output voltage and capacitor voltage quality. As a result, we continue the simulation with k_{out} = 0.2, k_c = 0.8 as optimal values. The higher impact of k_c proves the improved performance of the proposed iMPC compared to [50], in which the proposed cost function includes just k_{out}.

Figure 9 shows the simulation of the whole system under different load conditions with k_{out} = 0.2, k_c = 0.8. It includes an idle mode, a simple resistive load, and a nonlinear load. They are utilized in this case. This figure demonstrates the steady-state pictures with a better resolution as well as the dynamic behavior of the main grid, ac output, and the capacitor. This figure shows that the proposed iMPC can work because the THD of the output voltage and the grid current are in the range that they should be.

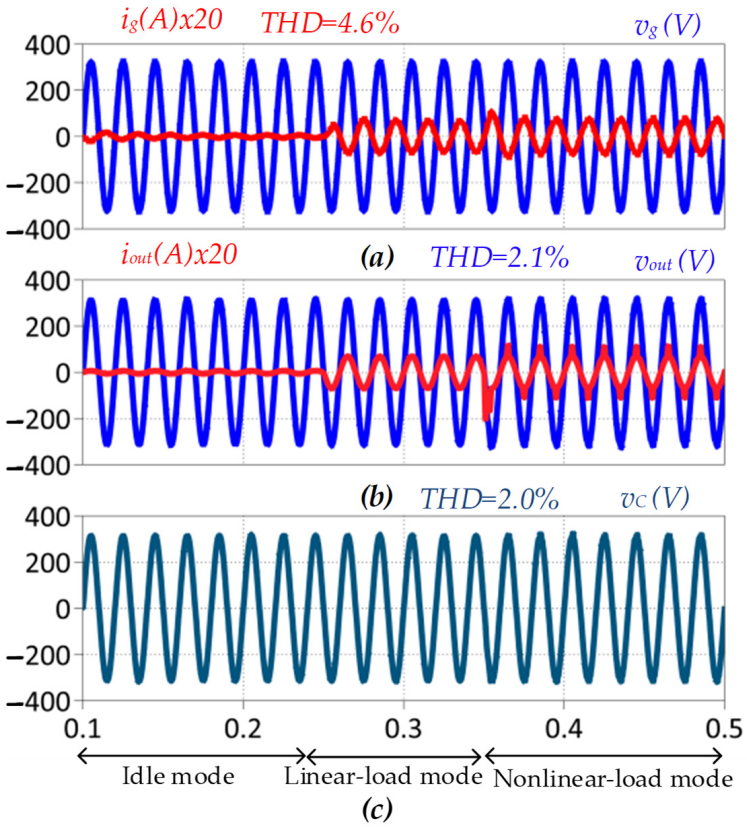

Figure 9. Voltage and current shape transitions at the main grid (**a**), output (**b**), and filter capacitor (**c**) with k_{out} = 0.2 and k_c = 0.8 in idle mode, linear load, and nonlinear load.

The next scenario evaluates the iMPC performance in the opposite power flow in a low-power solar microinverter connection. Figure 10 demonstrates the simulation results in idle mode with a current-source connection. The results confirm the good performance of the iMPC in terms of grid-forming. However, the high THD of the grid current implies the necessity of improvements in current control on the VSI1 side. The last case is the most complex and reveals a problem with any grid configured by power electronics. The high switching frequency current harmonics fluctuate between the ER and the microinverter.

The next level is the robustness evaluation of the proposed iMPC. As the grid-forming inverter mmust also work in droop control in the case of multiple loads and sources connection, the proposed control technique needs to be capable of tracking voltage with step changes. As a result, we test the iMPC performance in this case. In this scenario, we make a step-change in the reference value of the output voltage peak from 325 V to 305 V. The grid voltage and current, load voltage and current and filter capacitor voltage are depicted in Figure 11. In this case, gird current THD is 4.8%, however the iMPC provides voltage with THD of 2.2%. The total simulation results, in terms of the THD, are summarized in Table 2.

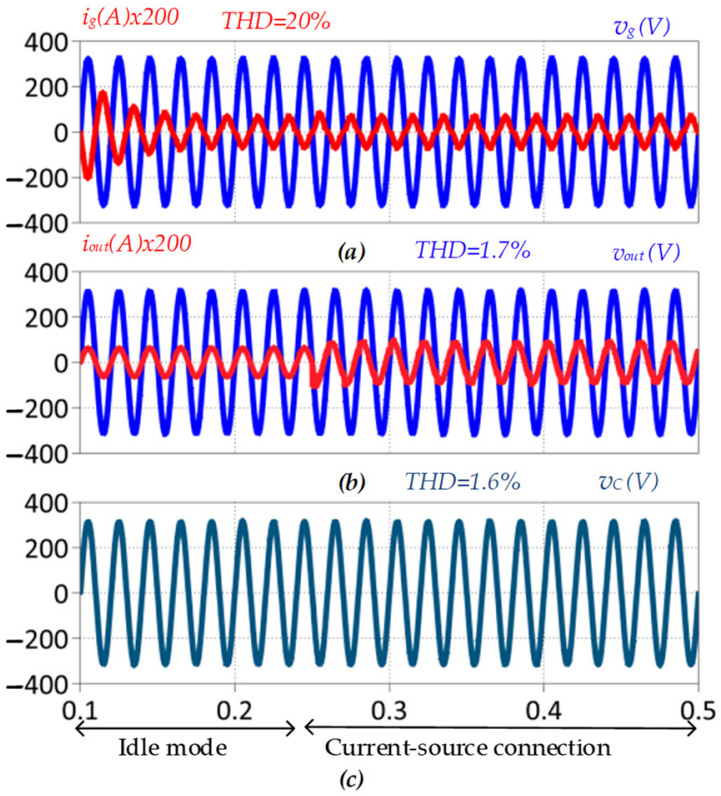

Figure 10. Voltage and current shape transition at the main grid (**a**), output (**b**), capacitor of the filter (**c**) with k_{out} = 0.2, k_c = 0.8 in idle mode, and current-source connection.

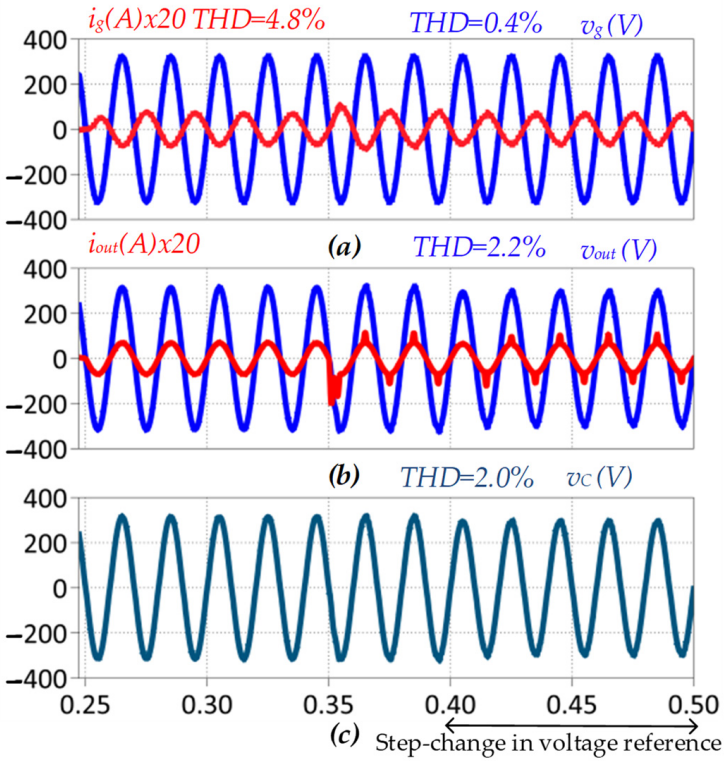

Figure 11. Voltage and current shape at the main grid (**a**), output (**b**), and capacitor of the filter (**c**) in case of drop voltage reference with k_{out} = 0.2, k_c = 0.8.

Table 2. Comparison of THD results of the ER parameters for different scenarios.

Scenario	Parameter	THD (%)
linear and nonlinear load with k_{out} = 0.0 and k_c = 1.0	Grid current i_g	4.6
	Output voltage v_{out}	2.1
	Filter capacitor voltage v_c	2.0
linear and nonlinear load with k_{out} = 1.0 and k_c = 0.0	Grid current i_g	4.6
	Output voltage v_{out}	2.4
	Filter capacitor voltage v_c	2.3
linear and nonlinear load with k_{out} = 0.2 and k_c = 0.8	Grid current i_g	4.6
	Output voltage v_{out}	2.1
	Filter capacitor voltage v_c	2.0
current-source connection with k_{out} = 0.2 and k_c = 0.8	Grid current ig	20
	Output voltage vout	1.7
	Filter capacitor voltage vc	1.6
Step change in reference from 230 V to 210 V with k_{out} = 0.2 and k_c = 0.8	Grid current i_g	4.8
	Output voltage v_{out}	2.2
	Filter capacitor voltage v_c	2.0

It can be seen that the proposed control approach is capable of maintaining the sinusoidal voltage in the PCC under any type of load that can be connected on the house side. Moreover, it underlines that the ER requires modification on the VSI1 side to maintain an acceptable quality of the injected current on the local grid under any load from the consumer side. Finally, bidirectional operation is possible without significant PCC voltage distortion.

5. Conclusions

This work studies the energy-router-based back-to-back inverter in grid-forming mode. The conventional PR regulator for grid-forming of the energy router has limitations in terms of its idle mode, nonlinear loads and current sources. This paper proposes an enhanced iMPC to improve the output voltage quality of the energy router. To improve the THD of the output voltage, a prediction horizon of two is suggested. Increasing the number of voltage deviations in each horizon will improve the output voltage quality at the expense of a higher processing burden on the microcontroller at each sampling time. Considering this issue, a voltage deviation of five is implemented, with a total of 25 loops in each sampling time. The simulation results for four different modes of idle mode, linear load, nonlinear load, and low-power current source show the higher impact of filter capacitor voltage on the THD of the output voltage. The results confirm that the proposed technique can control the steady-state and dynamic performance of the energy router in a grid-forming operation. In addition, the high THD of the grid current in the current-source connection proves the necessity of improvements in grid-following side control of the ER.

Future research can be conducted regarding the experimental verification of the proposed technique in different operation scenarios.

Author Contributions: Conceptualization: R.S.; Formal analysis: N.S. and M.N.; Validation: M.N. and N.S.; Methodology: O.H.; Visualization M.N., I.R. and K.N.; Investigation: M.N. and N.S.; Writing—original draft; M.N. and K.N.; Resources: I.R. and K.N.; Writing—review and editing: R.S. and D.V.; Supervision: D.V. and O.H.; Project administration: R.S.; Funding acquisition: N.S. All authors have read and agreed to the published version of the manuscript.

Funding: The project is financed by the "program of the Ministry of Science and Higher Education "Regional Excellence Initiative" in the years 2019–2022 project number 006/RID/2018/19 grant amount 11,870,000 PLN", realized in the GDYNIA MARITIME UNIVERSITY, POLAND.

Institutional Review Board Statement: Not applicable.

Informed Consent Statement: Not applicable.

Data Availability Statement: Not applicable.

Conflicts of Interest: The authors declare no conflict of interest.

References

1. Liu, Y.; Fang, Y.; Li, J. Interconnecting microgrids via the energy router with smart energy management. *Energies* **2017**, *10*, 1297. [CrossRef]
2. Huang, A.Q.; Crow, M.L.; Heydt, G.T.; Zheng, J.P.; Dale, S.J. The future renewable electric energy delivery and management (FREEDM) system: The energy internet. *Proc. IEEE* **2011**, *99*, 133–148. [CrossRef]
3. Roncero-Clemente, C.; Vilhena, N.; Delgado-Gomes, V.; Romero-Cadaval, E.; Martins, J.F. Control and operation of a three-phase local energy router for prosumers in a smart community. *IET Renew. Power Gener.* **2020**, *14*, 560–570. [CrossRef]
4. Martins, J.F.; Romero-Cadaval, E.; Vinnikov, D.; Malinowski, M. Transactive Electronics Power Energy: Challenges. *IEEE Power Electron. Mag.* **2022**, *9*, 20–32. [CrossRef]
5. Liu, Y.; Li, J.; Wu, Y.; Zhou, F. Coordinated Control of the Energy Router-Based Smart Home Energy Management System. *Appl. Sci.* **2017**, *7*, 943. [CrossRef]
6. Fu, R.; Remo, T.; Margolis, R.; Fu, R.; Remo, T.; Margolis, R. 2018 U.S. Utility-Scale Photovoltaics-Plus-Energy Storage System Costs Benchmark. 2018. Available online: https://www.nrel.gov/docs/fy19osti/71714.pdf.%0Ahttps://www.nrel.gov/docs/fy19osti/71714.pdf (accessed on 21 November 2018).
7. Liu, Y.; Chen, X.; Wu, Y.; Yang, K.; Zhu, J.; Li, B. Enabling the Smart and Flexible Management of Energy Prosumers via the Energy Router with Parallel Operation Mode. *IEEE Access* **2020**, *8*, 35038–35047. [CrossRef]
8. Liu, Y.; Li, Y.; Liang, H.; He, J.; Cui, H. Energy Routing Control Strategy for Integrated Microgrids Including Photovoltaic, Battery-Energy Storage and Electric Vehicles. *Energies* **2019**, *12*, 302. [CrossRef]
9. Ray, O.; Mishra, S. Integrated Hybrid Output Converter as Power Router for Renewable-based Nanogrids. In Proceedings of the ECON 2015—41st Annual Conference of the IEEE Industrial Electronics Society, Yokohama, Japan, 9–12 November 2015; pp. 1645–1650.
10. Zhen, L.; Penghua, L.; Wanxing, S.; Songhuai, D.; Qing, D.; Zhipeng, L. Research on a household energy router for energy internet. In Proceedings of the 2018 13th IEEE Conference on Industrial Electronics and Applications (ICIEA), Wuhan, China, 31 May–2 June 2018; pp. 952–957. [CrossRef]
11. Tarafdar, M.H.; Hamzeh, F. Aghdam Smart Hybrid Nanogrids Using Modular Multiport Power Electronic Interface. In Proceedings of the 2016 IEEE Innovative Smart Grid Technologies—Asia (ISGT-Asia), Melbourne, VIC, Australia, 28 November–1 December 2016; pp. 11–16.
12. Mishra, S.; Ray, O. Advances in nanogrid technology and its integration into rural electrification in India. In Proceedings of the 2014 International Power Electronics Conference (IPEC-Hiroshima 2014—ECCE ASIA), Hiroshima, Japan, 18–21 May 2014; pp. 2707–2713. [CrossRef]
13. Majumder, R. A hybrid microgrid with dc connection at back to back converters. *IEEE Trans. Smart Grid* **2014**, *5*, 251–259. [CrossRef]
14. Najafzadeh, M.; Husev, O.; Roasto, I.; Jalakas, T. Improved DC-Link Voltage Transient Response and Stability Issues in Energy Router with Fuzzy Logic Control Method. In Proceedings of the 2020 IEEE 61th International Scientific Conference on Power and Electrical Engineering of Riga Technical University (RTUCON), Riga, Latvia, 5–7 November 2020.
15. Roasto, I.; Rosin, A.; Jalakas, T. Multiport Interface Converter with an Energy Storage for Nanogrids. In Proceedings of the IECON 2018—44th Annual Conference of the IEEE Industrial Electronics Society, Washington, DC, USA, 21–23 October 2018; Volume 1, pp. 6088–6093.
16. Najafzadeh, M.; Roasto, I.; Jalakas, T. Energy Router Based Energy Management System for Nearly Zero Energy Buildings. In Proceedings of the 2019 IEEE 60th International Scientific Conference on Power and Electrical Engineering of Riga Technical University (RTUCON), Riga, Latvia, 7–9 October 2019.
17. Yang, Y.; Hadjidemetriou, L.; Blaabjerg, F.; Kyriakides, E. Benchmarking of Phase Locked Loop based Synchronization Techniques for Grid-Connected Inverter Systems. In Proceedings of the 9th International Conference on Power Electronics—ECCE Asia, Seoul, Korea, 1–5 June 2015; pp. 2167–2174.
18. Husev, O.; Roncero-Clemente, C.; Makovenko, E.; Pimentel, S.P.; Vinnikov, D.; Martins, J. Optimization and Implementation of the Proportional-Resonant Controller for Grid-Connected Inverter with Significant Computation Delay. *IEEE Trans. Ind. Electron.* **2020**, *67*, 1201–1211. [CrossRef]
19. Rocabert, J.; Luna, A.; Blaabjerg, F.; Rodriguez, P. Control of Power Converters in AC Microgrids. *IEEE Trans. Power Electron.* **2012**, *27*, 4734–4749. [CrossRef]
20. Hossain, M.J.A.J.; Pota, H.R.; Issa, W.; Hossain, M.J.A.J. Overview of AC microgrid controls with inverter-interfaced generations. *Energies* **2017**, *10*, 1300. [CrossRef]
21. Unamuno, E.; Barrena, J.A. Hybrid ac/dc microgrids—Part II: Review and classification of control strategies. *Renew. Sustain. Energy Rev.* **2015**, *52*, 1123–1134. [CrossRef]
22. Malik, S.M.; Ai, X.; Sun, Y.; Zhengqi, C.; Shupeng, Z. Voltage and frequency control strategies of hybrid AC/DC microgrid: A review. *IET Gener. Transm. Distrib.* **2017**, *11*, 303–313. [CrossRef]

23. Loh, P.C.; Li, D.; Chai, Y.K.; Blaabjerg, F. Autonomous control of interlinking converter with energy storage in hybrid AC-DC microgrid. *IEEE Trans. Ind. Appl.* **2013**, *49*, 1374–1382. [CrossRef]
24. Tayab, U.B.; Roslan, M.A.B.; Hwai, L.J.; Kashif, M. A review of droop control techniques for microgrid. *Renew. Sustain. Energy Rev.* **2017**, *76*, 717–727. [CrossRef]
25. Guerrero, J.M.; de Vicuña, L.G.; Matas, J.; Castilla, M. Output Impedance Design of Parallel-Connected UPS Inverters with Wireless Load-Sharing Control. *IEEE Trans. Ind. Electron.* **2005**, *52*, 1126–1135. [CrossRef]
26. Zhang, H.; Zhou, J.; Sun, Q.; Guerrero, J.M.; Ma, D. Data-Driven Control for Interlinked AC/DC Microgrids Via Model-Free Adaptive Control and Dual-Droop Control. *IEEE Trans. Smart Grid* **2017**, *8*, 557–571. [CrossRef]
27. Mahmood, H.; Michaelson, D.; Jiang, J. Decentralized Power Management of a PV/Battery Hybrid Unit in a Droop-Controlled Islanded Microgrid. *IEEE Trans. Power Electron.* **2015**, *30*, 7215–7229. [CrossRef]
28. Wang, J.; Dong, C.; Jin, C.; Lin, P.; Wang, P. Distributed Uniform Control for Parallel Bidirectional Interlinking Converters for Resilient Operation of Hybrid AC/DC Microgrid. *IEEE Trans. Sustain. Energy* **2022**, *13*, 3–13. [CrossRef]
29. He, J.; Li, Y.W.; Guerrero, J.M.; Blaabjerg, F.; Vasquez, J.C. An Islanding Microgrid Power Sharing Approach Using Enhanced Virtual Impedance Control Scheme. *IEEE Trans. Power Electron.* **2013**, *28*, 5272–5282. [CrossRef]
30. Jiang, X.y.; He, C.; Jermsittiparsert, K. Online optimal stationary reference frame controller for inverter interfaced distributed generation in a microgrid system. *Energy Rep.* **2020**, *6*, 134–145. [CrossRef]
31. Zhong, Q.C.; Weiss, G. Synchronverters: Inverters that mimic synchronous generators. *IEEE Trans. Ind. Electron.* **2011**, *58*, 1259–1267. [CrossRef]
32. Liu, J.; Hossain, M.J.; Lu, J.; Rafi, F.H.M.; Li, H. A hybrid AC/DC microgrid control system based on a virtual synchronous generator for smooth transient performances. *Electr. Power Syst. Res.* **2018**, *162*, 169–182. [CrossRef]
33. Arghir, C.; Jouini, T.; Dörfler, F. Grid-forming control for power converters based on matching of synchronous machines. *Automatica* **2018**, *95*, 273–282. [CrossRef]
34. Wang, J.; Rong, J.; Yu, L. Dynamic prescribed performance sliding mode control for DC–DC buck converter system with mismatched time-varying disturbances. *ISA Trans.* 2022; *in press*. [CrossRef]
35. Wang, J.; Rong, J.; Yang, J. Adaptive Fixed-Time Position Precision Control for Magnetic Levitation Systems. *IEEE Trans. Autom. Sci. Eng.* **2022**, 1–12. [CrossRef]
36. Kouro, S.; Perez, M.A.; Rodriguez, J.; Llor, A.M.; Young, H.A. Model Predictive Control: MPC's Role in the Evolution of Power Electronics. *IEEE Ind. Electron. Mag.* **2015**, *9*, 8–21. [CrossRef]
37. Rodriguez, J.; Kolar, J.; Espinoza, J.; Rivera, M.; Rojas, C. Predictive Torque and Flux Control of an Induction Machine fed by an Indirect Matrix Converter with Reactive Power Minimization. In Proceedings of the 2010 IEEE International Symposium on Industrial Electronics, Bari, Italy, 4–7 July 2010; pp. 3177–3183.
38. Kennel, R.; Linder, A. Predictive control of inverter supplied electrical drives. In Proceedings of the 2000 IEEE 31st Annual Power Electronics Specialists Conference. Conference Proceedings (Cat. No. 00CH37018), Galway, Ireland, 23 June 2000; pp. 761–766.
39. Zhuikov, V.; Pavlov, V.; Strzelecki, R.G. *Preemptive Control Systems for Valve Converters*; Nauk. Dumka: Kiev, Ukraine, 1991; 240p.
40. Rodriguez, J.; Kazmierkowski, M.P.; Espinoza, J.R.; Zanchetta, P.; Abu-Rub, H.; Young, H.A.; Rojas, C.A. State of the art of finite control set model predictive control in power electronics. *IEEE Trans. Ind. Inform.* **2013**, *9*, 1003–1016. [CrossRef]
41. Falkowski, P.; Sikorski, A. Finite Control Set Model Predictive Control for Grid-Connected AC—DC Converters with LCL Filter. *IEEE Trans. Ind. Electron.* **2018**, *65*, 2844–2852. [CrossRef]
42. Wojciechowski, D.; Strzelecki, R. Sensorless predictive control of three-phase parallel active filter. In Proceedings of the AFRICON 2007, Windhoek, South Africa, 26–28 September 2007.
43. Hu, J.; Shan, Y.; Guerrero, J.M.; Ioinovici, A.; Chan, K.W.; Rodriguez, J. Model predictive control of microgrids–An overview. *Renew. Sustain. Energy Rev.* **2021**, *136*, 110422. [CrossRef]
44. Wojciechowski, M.; Strzelecki, R.; Benysek, G. Predictive Control System of the Shunt Active Power Filter. In Proceedings of the 2008 International Biennial Baltic Electronics Conference (BEC2008), Tallinn, Estonia, 6–8 October 2008.
45. Wojciechowski, D.; Strzelecki, R. Predictive Control of Active Filter System with LCL Coupling Circuit. In Proceedings of the 2010 International Power Electronics Conference, Sapporo, Japan, 21–24 June 2010.
46. Lee, J.; Lee, J.; Moon, H.; Lee, K. An Improved Finite-Set Model Predictive Control Based on Discrete Space Vector Modulation Methods for Grid-Connected Three-Level Voltage Source Inverter. *IEEE J. Emerg. Sel. Top. Power Electron.* **2018**, *6*, 1744–1760. [CrossRef]
47. Wang, F.; Xie, H.; Chen, Q.; Davari, S.A.; Rodríguez, J.; Kennel, R. Parallel Predictive Torque Control for Induction Machines Without Weighting Factors. *IEEE Trans. Power Electron.* **2020**, *35*, 1779–1788. [CrossRef]
48. Wang, J.; Yang, H.; Liu, Y.; Rodriguez, J. Low-cost Multi-step FCS-MPCC for PMSM Drives Using a DC Link Single Current Sensor. *IEEE Trans. Power Electron.* **2022**, *37*, 11034–11044. [CrossRef]
49. Najafzadeh, M.; Ahmadiahangar, R.; Husev, O.; Roasto, I.; Jalakas, T.; Blinov, A. Recent Contributions, Future Prospects and Limitations of Interlinking Converter Control in Hybrid AC/DC Microgrids. *IEEE Access* **2021**, *9*, 7960–7984. [CrossRef]
50. Roasto, I.; Husev, O.; Najafzadeh, M.; Jalakas, T.; Rodriguez, J. Voltage Source Operation of the Energy-Router Based on Model Predictive Control. *Energies* **2019**, *12*, 1892. [CrossRef]